On the application of the volume free strain energy density method to blunt V-notches under mixed mode condition

Pietro Foti [a],[*], Seyed Mohammad Javad Razavi [a], Majid Reza Ayatollahi [b], Liviu Marsavina [c], Filippo Berto [a]

[a] Norwegian University of Science and Technology, MTP Gløshaugen, Richard Birkelands vei 2B, Trondheim 7491, Norway
[b] School of Mechanical Engineering, Iran University of Science and Technology, Narmak, 16846 Tehran, Iran
[c] University Politehnica Timisoara, Department Mechanics and Strength of Materials, Timisoara 300222, Romania

ARTICLE INFO

ABSTRACT

This work investigates the possibility to apply the strain energy density method, as regards blunt V-notches under mixed loading condition, through finite element models with a free mesh pattern. It is worth underlining that the conventional procedure for the application of this method to this kind of components requires two different numerical simulations. A first simulation is needed to define the point of maximum of the first principal stress field along the notch fillet whose position represents an input for a second simulation to build the control volume in the right position to apply the method. Several numerical analyses were carried out to compare the conventional procedure of the method with this new procedure that allows the application of the method as a post-processing tool. The main advantage of this new procedure applied to components without stress singularity is that, by accepting an error that depends on the mesh refinement, the efforts of designers and researchers and the calculation time are decreased. The error in evaluating the SED value has been found to have a zero average value with a standard deviation of 1% and a maximum absolute value of 4.5% having a ratio between the main geometrical parameters of the control volume and the average mesh size comprised in the following range $3 < min[R_0; \gamma/2]/Size_{averaged} \leq 5$. Dealing with this kind of components, the calculation time decreases by at least 50% requiring one simulation instead of the two requested by the conventional procedure.

1. Introduction

The fracture assessment, as well as the fatigue life predictions, are faced by designers and researchers dealing with civil structures and mechanical components to avoid unexpected and catastrophic failures that could also involve loss of lives. The need of feasible tools to evaluate with accuracy the material properties under both static and dynamic conditions is evident but nowadays they are still mostly assessed based on a method that generally leads to an excessively conservative design. Even if this is generally accepted because of the difficulties to perform a more precise assessment, it is undesirable in those mechanical fields that require a lightweight design such as automotive and aircraft engineering.

Dealing with welded joints, the failure assessment is usually demanded to global methods. The standards are mainly based on two global approaches: the nominal stress approach [1–3] that considers external loads or nominal stresses in the critical cross-section and compares them with the S-N curves that correlate the fatigue strength versus the number of cycles; the structural stress approach that considers the stress concentration effects of the component due to the global geometry [1–5] and allows the fatigue assessment using the structural stresses with an S-N curve that is independent on the particular type of weld and the geometry of the component.

These methods represent nowadays the base for fatigue assessment in almost all areas of mechanical and structural engineering due to their simplicity and statistical proof. However, they generally lead to an excessively conservative design and, since their validation is based on tests carried out on geometry and conditions rarely encountered in practical applications, the assessment of a generic mechanical component lacks actually a statistical validation [6]. A valid alternative is represented by the local approaches that are able to evaluate with more accuracy the mechanical properties of structural components [7–9]. Their major drawbacks are that they require expertise in their application and that a feasible application of these methods requires the
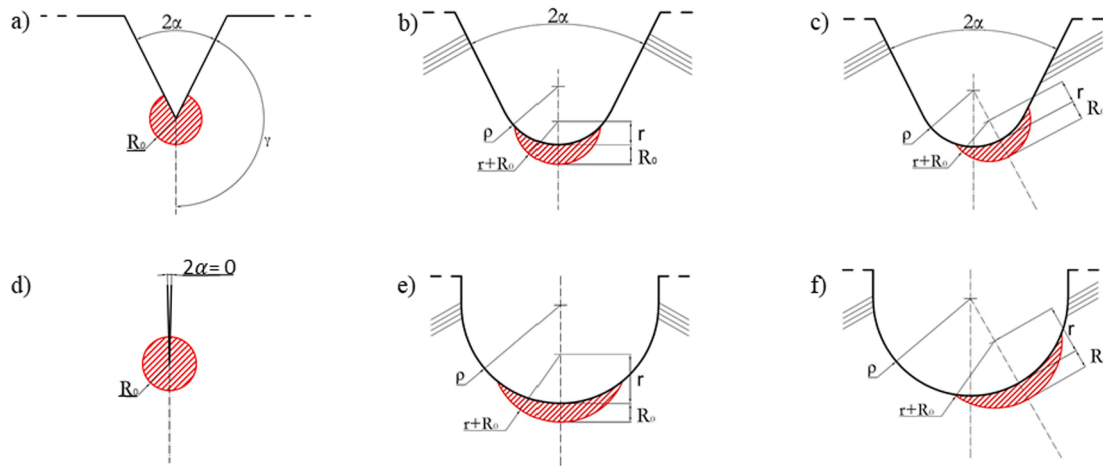
Fig. 1. Control volume for: (a) Sharp V-notch; (b) blunt V-notch under mode I loading; (c) blunt V-notch under mixed mode loading; (c) Crack; (d) U-notch under mode I loading; (e) U-notch under mixed mode loading.

determination of those parameters that have an incisive influence in the component behavior in order to avoid complicating, even more, the problem.

In this work, we focus on the Strain Energy Density (SED) method that has been validated as a method to investigate both fracture in static condition and fatigue failure [10–15].

One of the major drawbacks of this method is that requires a Finite Element (FE) model built in order to have a volume, called control volume, centered on the critical point of the components according to the theory of the method that is explained in section 2. The application of this method to components without stress singularity results also in two different numerical simulations making the method less attractive.

Following the researches of other authors [16–21], it became clear that an increasing interest has grown through the simplification of the method trying to avoid the construction of the control volume in the FE model and to exploit the SED method low sensitivity [22] to the mesh refinement in order to apply it using FE models with a free coarse mesh pattern. However, all the researches carried out with the purpose stated above are limited to components that present a stress singularity such as sharp V-notches and do not consider components with complex geometry whose assessment both in static and fatigue assessment could benefit from the application of the SED method.

In order to simplify the method with regards to its application to blunt V-notches, we evaluated the following points in this work:

- the possibility to estimate the SED value without the construction of the control volume in the pre-processing phase of the FEM code dealing with components containing blunt V-notches under mixed mode loading;
- the effect on the SED evaluation due to the error in evaluating the location of the maximum of the first principal stress field at the notch edge, an input needed to center the control volume in components without a stress singularity;
- the influence of different FE modeling parameters in order to establish some useful recommendations for the designers that want to apply the SED method according to the volume free procedure.

2. Strain Energy Density method

The SED method is an energetic local approach validated as a method to investigate both fracture in static condition and fatigue failure [10,11,14,23–27].

As regard the static condition, the method assumes that brittle fracture occurs when the local SED, W, averaged over a given control volume, reaches a critical value, $\overline{W} = W_C$, that results to be independent

on both the local geometry and the loading mode [10,11,28,29]. From a theoretical point of view, considering a material having a perfect brittle behavior, under static conditions, the mean SED critical value can be evaluated through the conventional ultimate tensile strength, σ_t, and the Young's modulus of the material:

$$W_C = \frac{\sigma_t^2}{2E} \tag{1}$$

What stated above represents the basic idea of this method, whose analytical frame [30–36] demonstrates also connections in closed form with other fracture mechanics methods such as the notch stress intensity factor.

Dealing with welded joints made of steel or aluminium [37–43], two conditions allow the use of the SED method to assess their high cycle fatigue properties in terms of the cyclic average SED, $\Delta\overline{W}$: the brittle nature of the failure and the fact that it happens under the linear elastic regime.

The first validation of the SED method, to assess the fatigue properties of welded joints, involved a study carried out on more than 300 fatigue test data with toe failure under different loading modes [37]. The analysis was later applied to a larger bulk of experimental data involving components with competing failure modes under different loading conditions, providing a final synthesis based on 900 experimental data [44], where the number of cycles is given as a function of the cyclic average SED.

Some more considerations should be done about the so-called control volume. This has a characteristic length, R_0, that is dependent on the material properties and is different dealing with static and dynamic loadings conditions [30]. Besides, the control volume shape (this does not include the characteristic length R_0) results to be dependent on both the local geometry and the loading conditions; indeed it takes different shapes with regard to the local geometry and different positions according to the loading mode as explained below.

As regards cracks and sharp V-notches in plane problems both in mode I and mixed mode loading, the control volume is a sector-shaped cylinder of radius R_0 with its axis along the notch tip line as shown in Fig. 1(a) for V-notch and in Fig. 1(d) for cracks.

Dealing with blunt notches [37,45–53], the control volume assumes a crescent moon shape, with R_0 being its maximum depth inside the component. In this case, the control volume is given by the intersection between the component and a circle of radius $r + R_0$, where $r = \rho(\pi - 2\alpha)/(2\pi - 2\alpha)$ [45], being 2α the notch opening angle and ρ the notch radius. The center of the control volume is not always located on the notch bisector, but on a line rigidly rotated with respect to it and centered on that point where the first principal stress fields reaches its

maximum value, following, essentially, the mode I dominance concept. The center of this circle is located between the notch edge and the notch-fitting radius center, at a distance r from the notch edge as shown in Fig. 1(b) and (c) for blunt V-notches and in Fig. 1(e) and (f) for U-notches. The need to know the position of the first principal stress maximum (FPSM), in order to locate the control volume, leads to two different numerical simulations to apply the SED method to components with this geometry.

The purpose of the present work is to evaluate the error in achieving the SED value for components without stress singularity, such as blunt V-notches, considering only one numerical simulation carried out though a model with a free mesh pattern built imposing only a refinement near the notch fitting curve according to a criterion explained in the next section.

3. Finite element analysis

The detail taken into account for this study is a flat, double V-notched, specimen with the notch bisectors lying on the same line that forms an angle β with the loading direction. The shape of this specimen allows to consider mixed mode loading conditions; indeed, with changing β, different contributions of mode I and mode II loading are achieved. Three different notch opening angles are considered, $[30°; 45°; 60°]$, while β assumes four different values, $[45°; 60°; 75°; 90°]$, and the notch fitting radius assumes five different values,

$[0.1; 0.5; 2; 4; 8]$mm. The specimens net section, calculated perpendicularly to the load application direction, is maintained constant while the notch fitting radius and the notch opening angle change.

As regards the SED evaluation, this was carried out considering five different values of the control volume radius $[0.2; 0.4; 0.6; 0.8; 1]$mm, five different mesh refinements and two different elements characterized by first and second order shape functions, respectively three-node PLANE 182 and six-node PLANE 183 in Ansys software, for each set of the geometrical parameters listed above. A comparison regarding the SED evaluation involving finite elements with different shape functions is also available in the literature [28] in regard to sharp V-notches revealing already low differences with changing the shape function of the used finite element. It is worth noting that the theoretical explanation given for the low sensitivity of SED to the mesh refinement [22] coupled with the purpose of the present work to assess the influence of variations in the integration domain, i.e. approximated control volume shape through selections of elements, make the authors assume a limited influence determined by the integration scheme exploited by the FE software. Considering that the expected error in evaluating the SED value is assessed without neglecting data coming from element selections that approximate very coarsely the control volume theoretical shape (see Fig. 6) resulting in conservative recommendations for applying the volume free procedure for the SED evaluation, the lower influence of the integration scheme exploited by the FE software could be considered covered in the present work.
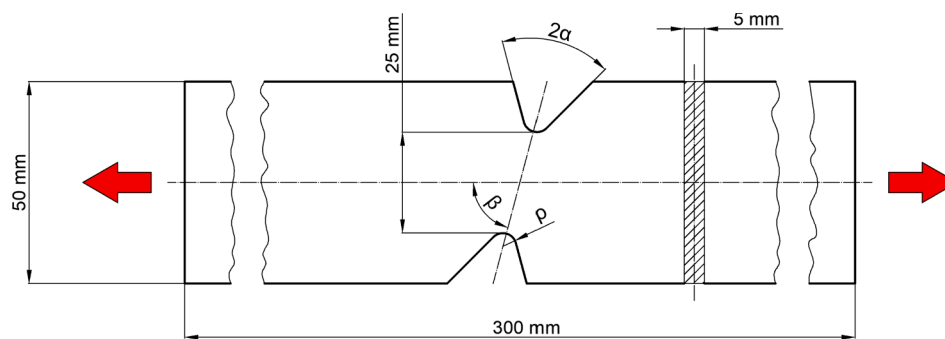
Fig. 2. Schematic representation of model geometry.
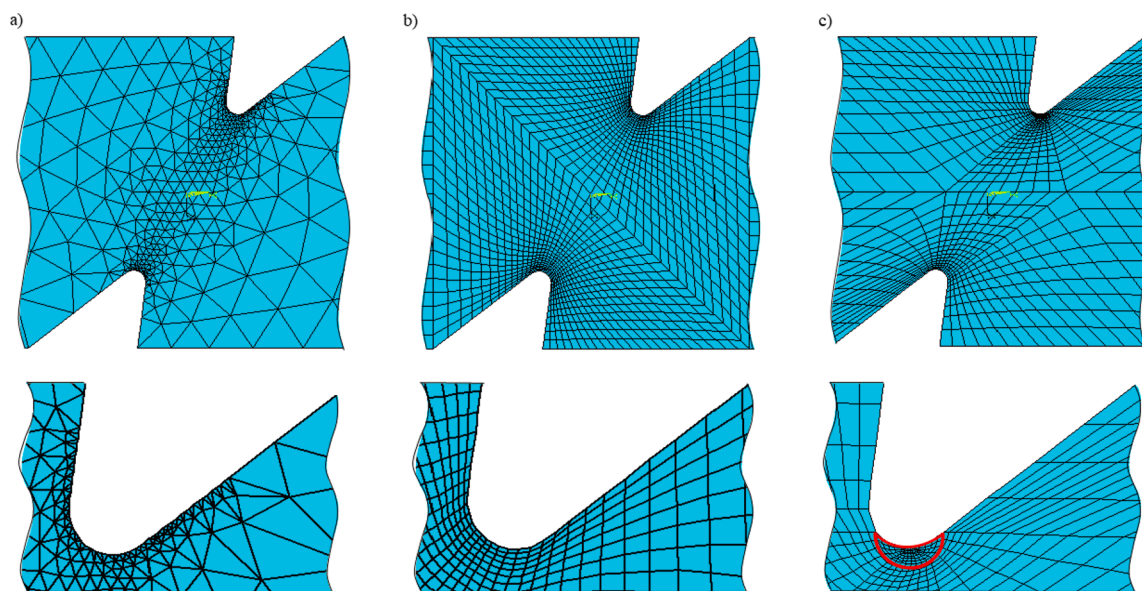
Fig. 3. FE models and particular of the notch tip zone discretization with: (a) free mesh for the application of the free volume SED (Model A); (b) mapped mesh to define the position of the first principal stress (Model B); (c) mapped mesh with control volume (marked in red) for the application of the conventional SED method (Model C). (For interpretation of the references to colour in this figure legend, the reader is referred to the web version of this article.)

This model, shown in Fig. 2, would require two different simulations for the application of the SED method; indeed, dealing with complex geometries that do not present a stress singularity like a sharp corner, there is the need to carry out the first simulation to evaluate the position of the FPSM that represents the input for a second simulation to build the control volume and apply the method. Three different models, shown in Fig. 3, are considered in the present study.

Model A has a completely free mesh realized imposing only the number of divisions along the notch fitting curve (see Fig. 3 a); the divisions are established as a fraction of half the notch fillet length $\gamma/2 = \rho \cdot (\pi - 2\alpha)/2$, shown in Fig. 5, or of the control volume radius R_0 when the following condition is satisfied $R_0 < \gamma/2$. Five different mesh refinements, defined as a fraction of R_0 or $\gamma/2$ and the size of the element, $size_{imp.}$, are considered according to the condition stated above: $[4; 8; 10; 15; 20]$.

Model B is built in order to have a mapped mesh pattern for the geometry considered but without the construction of the control volume (see Fig. 3b); this model is useful to evaluate the exact position of FPSM along the notch fitting curve whose value is taken as the reference to evaluate the accuracy of model A in estimating the position of the FPSM. Since this model is taken into account as a reference model, only one simulation, with a very refined mesh, is considered for each combination of the geometrical parameters.

Model C is represented by the conventional model built to evaluate the SED value with the construction of the control volume that uses as input the position of the FPSM acquired through the model B (see Fig. 3c). Model C, same as model B, is used only as a reference model to assess the error of model A.

The SED value has only been evaluated for models A and C. As regards the model A, the SED value is acquired through a selection of the elements using a polar coordinate system centered along the segment that links the point of FPSM and the center of curvature of the notch fitting curve at a distance r, whose value is assessed according to Fig. 1, from the component surface considering for the selection the following radial range: $[0; r + R_0]$. The result of such a selection is shown in Fig. 4 (a). As regards the model C, the SED value is acquired through the conventional procedure of the SED method leading to a control volume as shown in Fig. 4(b).

From Fig. 4(a) and (b), that show also the SED contour plot in the control volume for both the models shown in Fig. 3(a) and (c), it is possible to state that the new method to acquire the SED value stated above leads to a selection of the elements near the FPSM position that approximates very well the control volume built following the conventional procedure for the SED method.

4. Results and discussions

As stated above, the main aim of the present work is to evaluate the possibility to estimate the SED value with a free mesh model, dealing with components containing rounded V-notches under mixed mode loading that would require two different numerical simulations to apply the SED method following the conventional procedure of this method.

The application of the SED method to complex geometries is complicated by the need to establish the position of the FPSM in order to
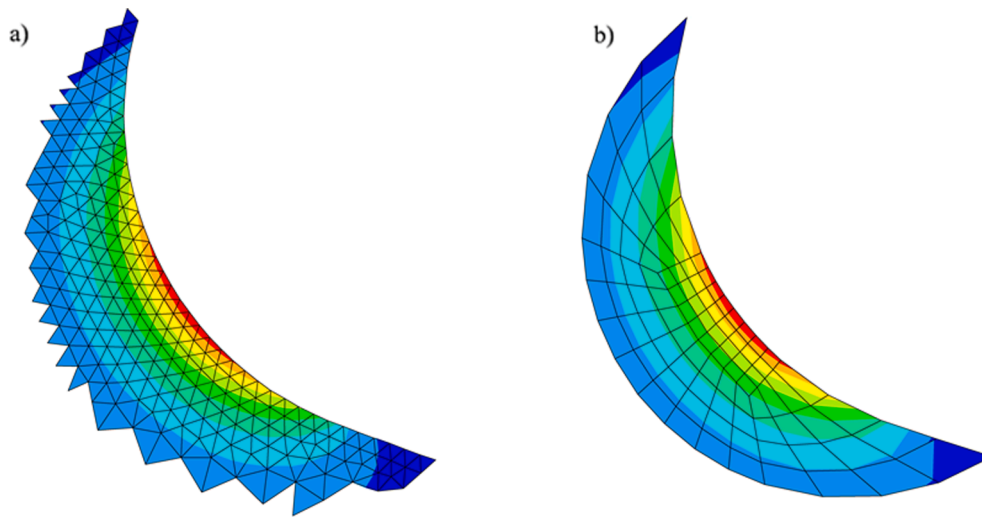

Fig. 4. Control volume and SED contour plot for: (a) Model A; (b) Model C.
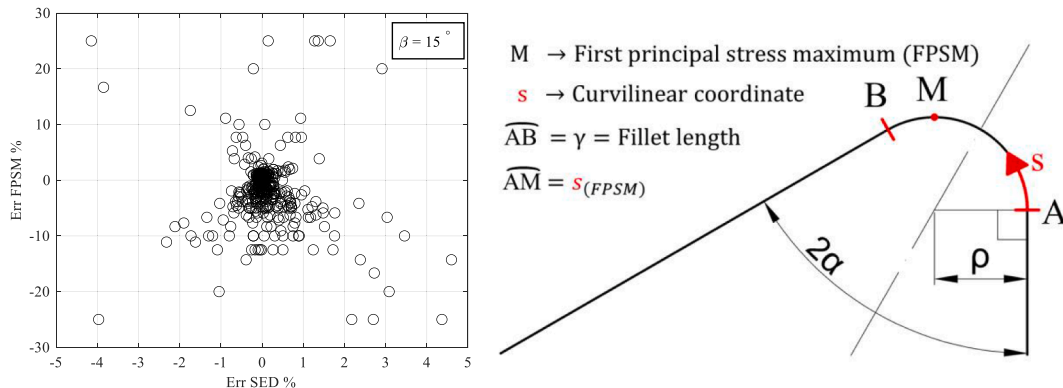

Fig. 5. Diagram reporting the error of the model A in evaluating the position of the FPSM vs the error in evaluating the SED value (left); curvilinear system of coordinate (right).

center the control volume in which the SED value is to be evaluated. The need to determine the stresses to know the right position for the control volume leads to the doubt that a very refined mesh is needed to compute exactly this position. In order to understand the effect that an imprecise evaluation of this point could have on the assessment of the SED value, we evaluated, through the model B, the position of the FPSM with a very refined mesh and we computed the error that the use of the model A could lead with its evaluation considering the analysed geometry in the present work. Since the position of the FPSM is characterized by two different coordinates of X and Y, it was decided to introduce a curvilinear coordinates system, shown in Fig. 5, in order to define the position of the FPSM with only one coordinate. In this way, it is possible to evaluate the error of this position through a single value. However, considering that the main aim of this work is to assess the error in evaluating the SED value, the authors were not interested in the error of the position itself but on the effect that this error could lead to the SED evaluation. We analysed the results with this purpose reporting in diagrams the error in the evaluation of the SED value vs the error in evaluating the position of the FPSM. Fig. 5 reports one of these diagrams that shows, for a fixed value of β and for models meshed with six-node PLANE 183 elements, the SED error vs the FPSM position error for all the possible combinations of the geometrical parameters listed in section 3.

From the diagram, it is evident that bigger error values in evaluating the position of the FPSM lead to smaller errors in evaluating the SED value. In the most cases, a small error for the SED value is associated with a small error in the FPSM position value but some cases lead to low error for the SED value even with a bigger error in the position value. It was not possible to establish whether a relation between the two errors was possible, but, considering that the position of the FPSM is not known a priori, such a relation would have been not useful for the purpose of this work. The same considerations are possible considering all the other

combinations of β and element types in the present work.

It is worth underlining that the different mesh refinements reported in section 3 represent only the imposed mesh size at the notch fillet but they do not reflect well the mesh size obtained within the elements selection; indeed, no convergence of the FE solution is reached with increasing the imposed mesh refinement. This is due to the fact that the imposed mesh size at the fillet does not take into account the mesh pattern of the elements selections. A simple solution to consider also the mesh pattern, according to the authors, is to take into account an average mesh size, $size_{ave}$, inside the control volume making the assumption that the elements have a perfect equilateral triangle shape. An example of the problem stated above is reported in Fig. 6(c) that shows the elements selection that has the greatest difference between the imposed mesh size and the averaged mesh size obtained.

Considering the large amount of acquired data through the numerical simulations, we report in tables, for each combination of β and average mesh refinement inside the control volume, the mean error, μ, the standard deviation, σ, and also the maximum and minimum errors achieved for the combination of all the other parameters considered in the present work. Table 1 reports the values for the six-node PLANE 183 elements while Table 2 reports the values for the three-node PLANE 182 elements.

From Tables 1 and 2, it is possible to notice that: the use of the element PLANE 183 leads to an average error of zero with a low standard deviation and maximum error achieved of almost 8% in absolute value; the use of the element PLANE 182 with three nodes usually leads to a negative average value that decreases, in absolute value, going from mixed mode conditions to mode I condition ($\beta = 90°$). The better estimation of the SED value given by the PLANE 183 element is better appreciable through Fig. 7 that reports the mean error, μ, and the standard deviation, σ, with changing β and the mesh refinement for all the combination of 2α and element type. The decreasing mean value of
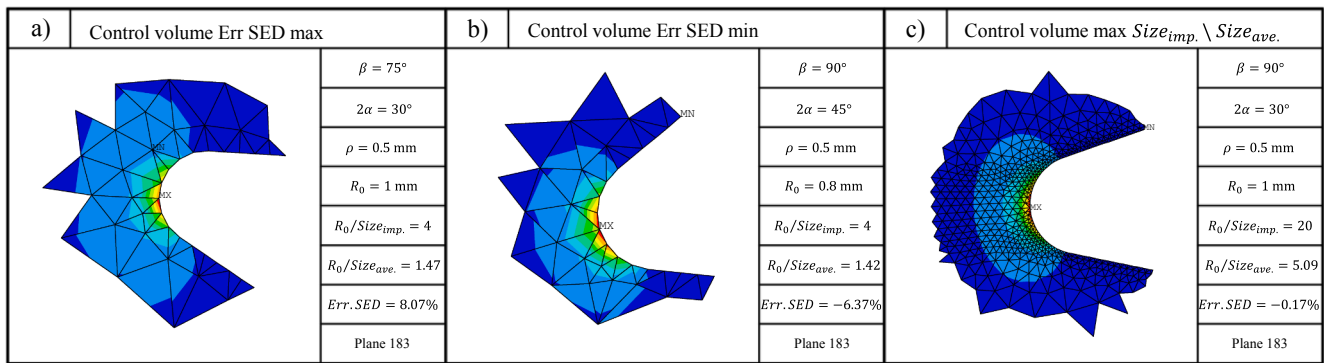

a)	Control volume Err SED max		b)	Control volume Err SED min		c)	Control volume max $Size_{imp.} \setminus Size_{ave.}$	
		$\beta = 75°$			$\beta = 90°$			$\beta = 90°$
		$2\alpha = 30°$			$2\alpha = 45°$			$2\alpha = 30°$
		$\rho = 0.5$ mm			$\rho = 0.5$ mm			$\rho = 0.5$ mm
		$R_0 = 1$ mm			$R_0 = 0.8$ mm			$R_0 = 1$ mm
		$R_0/Size_{imp.} = 4$			$R_0/Size_{imp.} = 4$			$R_0/Size_{imp.} = 20$
		$R_0/Size_{ave.} = 1.47$			$R_0/Size_{ave.} = 1.42$			$R_0/Size_{ave.} = 5.09$
		$Err.SED = 8.07\%$			$Err.SED = -6.37\%$			$Err.SED = -0.17\%$
		Plane 183			Plane 183			Plane 183

Fig. 6. Control volume mesh for: (a) maximum error achieved; (b) minimum error achieved; (c) maximum difference between the mesh size imposed and the average mesh size.

**Table 1**
Error % for element PLANE 183.

$\dfrac{\min[R_0;\gamma/2]}{Size_{averaged}}$	β															
	$45°$				$60°$				$75°$				$90°$			
	μ	σ	Max	Min	μ	σ	Max	Min	μ	σ	Max	Min	μ	σ	Max	Min
$1.10 < ratio \leq 3$	0.43	2.12	6.92	−4.24	0.18	1.93	6.62	−3.05	0.51	2.36	8.07	−5.65	0.24	1.66	4.60	−6.37
$3 < ratio \leq 5$	−0.16	1.15	4.44	−4.40	−0.14	0.70	2.18	−2.39	0.07	0.83	3.04	−1.99	0.06	0.76	3.62	−1.33
$5 < ratio \leq 7$	0.13	0.63	2.91	−2.41	−0.07	0.56	1.72	−1.83	0.17	0.61	2.00	−1.35	0.04	0.47	1.75	−1.36
$7 < ratio \leq 9$	−0.03	0.49	1.30	−2.04	0.03	0.40	1.17	−1.43	0.09	0.33	1.70	−0.70	0.04	0.31	1.67	−0.58
$9 < ratio \leq 11$	0.04	0.38	1.60	−1.25	0.03	0.45	1.66	−1.26	0.06	0.33	1.63	−0.81	0.05	0.37	2.03	−1.38
$11 < ratio \leq 13$	0.09	0.32	1.14	−0.62	0.00	0.28	0.61	−0.81	0.11	0.32	1.39	−0.42	0.08	0.36	1.37	−0.71
$13 < ratio \leq 15$	0.07	0.16	0.36	−0.22	−0.03	0.23	0.50	−1.27	0.06	0.19	1.24	−0.43	0.01	0.27	1.04	−1.97
$ratio > 15$	0.12	0.14	0.45	−0.03	−0.02	0.09	0.09	−0.30	0.07	0.14	0.65	−0.24	0.05	0.11	0.46	−0.20

Table 2
Error % for element PLANE 182.

$\dfrac{\min[R_0;\gamma/2]}{Size_{averaged}}$	β															
	45°				60°				75°				90°			
	μ	σ	Max	Min	μ	σ	Max	Min	μ	σ	Max	Min	μ	σ	Max	Min
$1.67 < ratio \leq 3$	−3.27	2.62	4.29	−8.35	−1.06	2.22	2.73	−4.93	−0.64	2.76	5.86	−4.05	0.29	2.90	7.21	−3.71
$3 < ratio \leq 5$	−3.53	1.60	1.20	−9.01	−2.00	1.13	2.75	−7.10	−1.10	1.11	2.76	−4.22	−1.08	1.10	2.52	−5.08
$5 < ratio \leq 7$	−3.37	1.23	0.53	−6.69	−2.17	0.80	0.23	−4.76	−1.30	1.15	1.43	−3.69	−1.51	1.02	1.91	−4.42
$7 < ratio \leq 9$	−3.19	0.99	1.48	−5.86	−2.02	0.54	0.23	−4.24	−1.26	0.58	0.43	−3.58	−1.13	0.79	−0.05	−3.53
$9 < ratio \leq 11$	−3.04	0.85	0.11	−5.14	−1.99	0.57	−0.72	−3.40	−1.17	0.50	−0.01	−2.96	−0.92	0.68	0.01	−3.05
$11 < ratio \leq 13$	−3.03	0.62	−1.83	−5.24	−2.09	0.50	−0.99	−3.59	−1.67	0.63	−0.06	−3.47	−1.62	0.64	−0.60	−3.54
$13 < ratio \leq 15$	−2.78	0.86	−1.20	−5.02	−1.97	0.47	−0.68	−3.19	−1.08	0.55	0.59	−2.99	−0.91	0.66	0.66	−2.83
$ratio > 15$	−2.21	0.62	−1.03	−3.36	−1.89	0.37	−1.10	−2.87	−1.16	0.49	−0.04	−2.61	−0.93	0.66	−0.02	−2.93
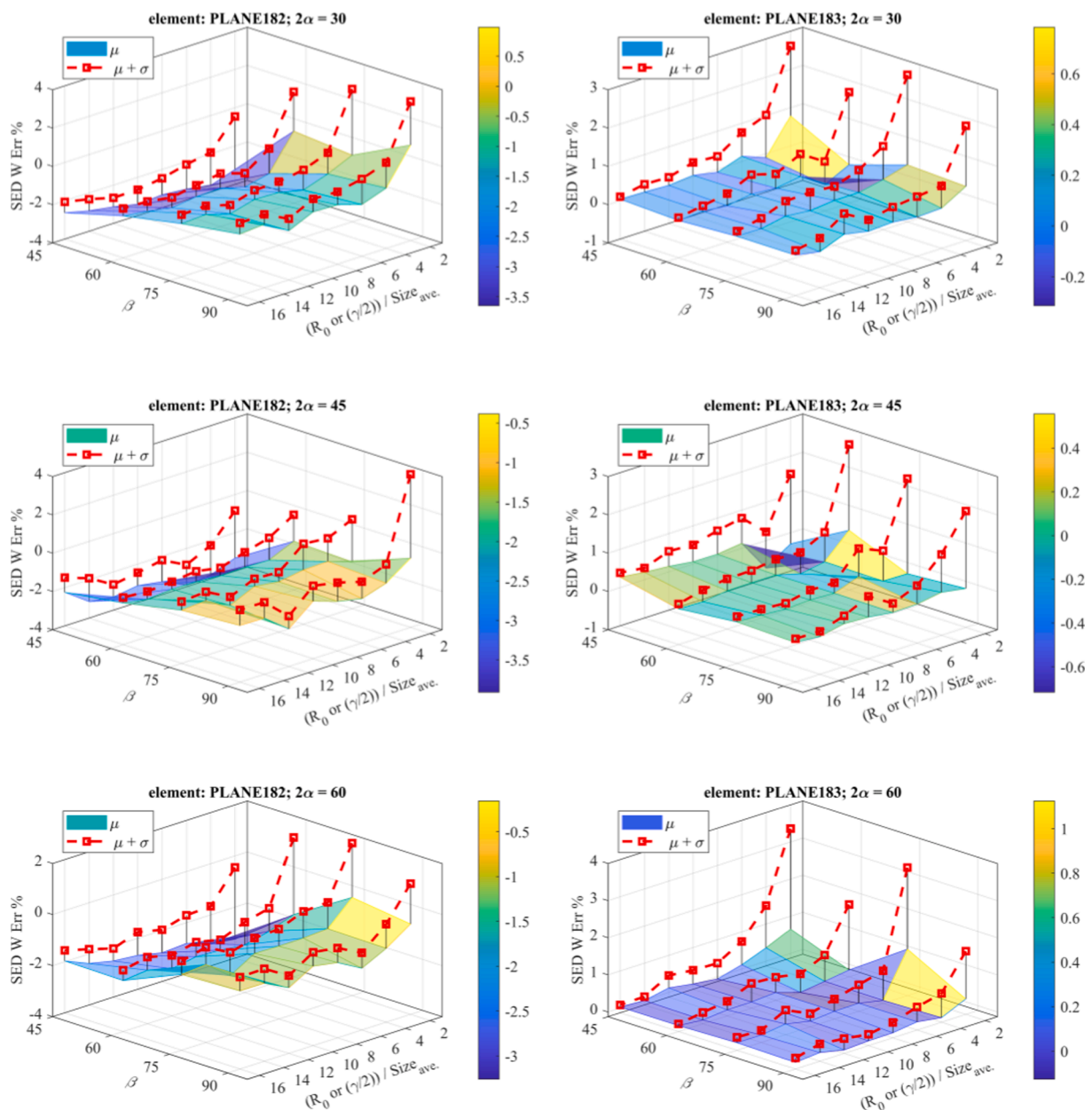
Fig. 7. Mean value, μ, and standard deviation, σ, of the error in evaluating the SED with changing β and mesh refinement for different notch opening angle 2α and element utilised in the FE analysis.

a)

b)
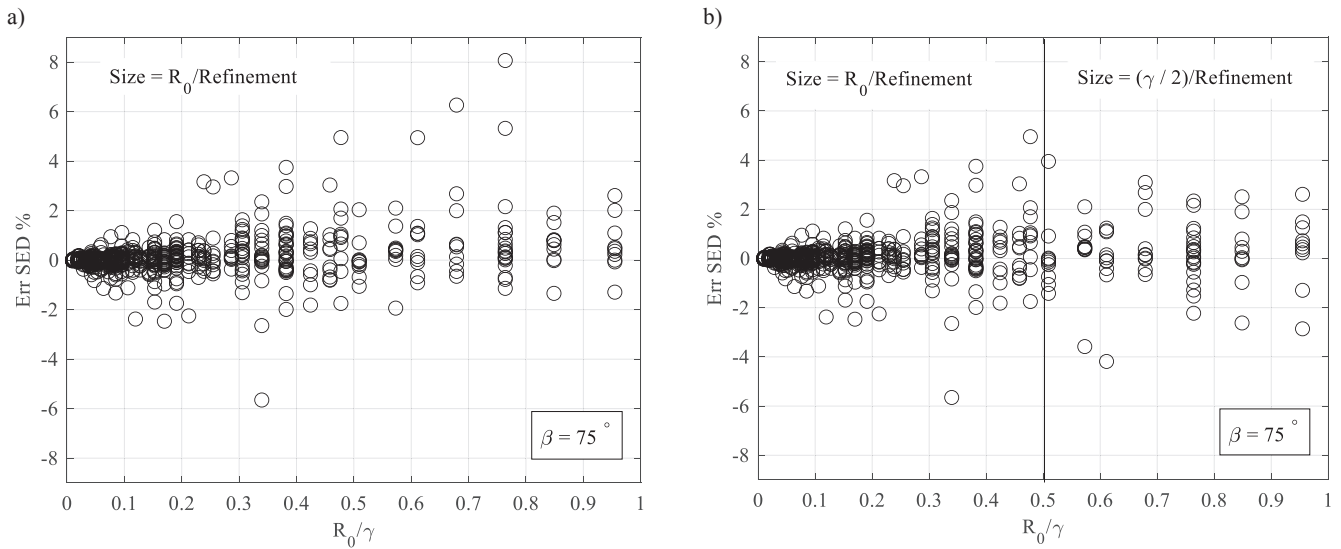
Fig. 8. Error SED W % vs ratio R_0/γ considering: (a) a mesh size of $R_0/Refinement$; a mesh size of $R_0/Refinement$ if $R_0/\gamma < 0.5$ and a mesh size of $(\gamma/2)/Refinement$ if.$R_0/\gamma \geq 0.5$
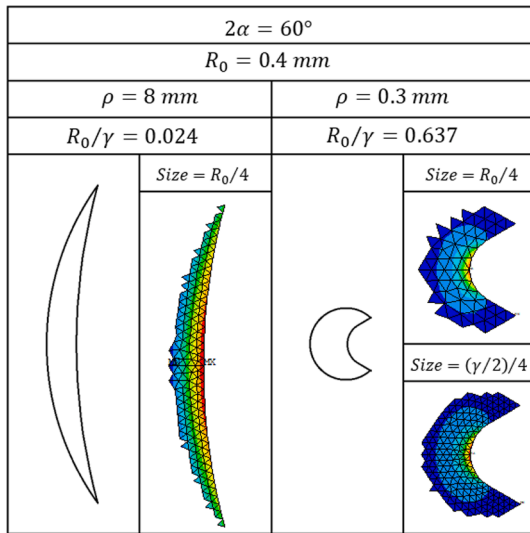
Fig. 9. Control volume shape and mesh with changing the ratio R_0/γ and the meshing criteria utilised to realise the model A.

the error, μ, with increasing β reflects the bad capability of the three-node PLANE182 element to simulate mixed mode problems. However, it is worth underlining that the use of the PLANE 182 element could lead to acceptable results in terms of SED decreasing even more the computational time required; this depends of course on the accuracy required by the application considered. As regards the standard deviation, the use of the two different elements does not lead to huge differences while, as regards the maximum and minimum values, it is possible to notice that the use of the PLANE 182 element could lead also to an underestimation of the SED value of -9%.

However, it is worth underlining that high values of the error in absolute value are related to a bad element selection due to the mesh pattern, as shown in Fig. 6 (a) and (b). A qualitative check to the shape of the selection in order to understand how much it deviates from the theoretical shape of the control volume help avoiding huge errors in the estimation.

An interesting relationship has been found between the error in evaluating the SED W and the ratio between the control volume radius and the fillet length, R_0/γ. In particular, the error in evaluating the SED

decreases with decreasing the ratio R_0/γ as presented in the diagrams reported in Fig. 8 that shows the effects of the mesh criteria considered in the present work. According to the authors, the decreasing error in evaluating the SED with decreasing the ratio R_0/γ could be addressed to the fact that, with low ratio of R_0/γ, the two arcs that define the control volume for this kind of geometry are much greater than R_0 and, being the mesh size a ratio of R_0, the selection of elements performed to evaluate the SED for model A is able to give a better approximation of the control volume shape leading to a lower error in the SED evaluation. For values of the ratio R_0/γ greater than 0.5 a mesh size defined as a ratio of $\gamma/2$ leads to a lower error in evaluating the SED. The mean value μ and the standard deviation σ of the error in evaluating the SED value are almost unchanged but a greater effect has been detected as regards the maximum error achieved through the simulations carried out.

Fig. 9 reports also two different examples of the control volume. In particular, the one on the right shows how the mesh changes according to the meshing criterion established in section 3; Indeed, as regards the control volume characterized by a ratio $R_0/\gamma = 0.637$, it is possible to appreciate the better approximation of the control volume shape given by a mesh size of $(\gamma/2)/4$ instead of $R_0/4$.

5. Conclusions

The possibility to evaluate the SED value through a free mesh FE model is investigated in the present work in order to simplify the SED method as regards its application to complex geometries under mixed loading conditions that would require two different FE simulations to assess the SED value through the conventional procedure of the method. Several numerical analyses have been carried out for three different FE models with changing several geometrical parameters, control volume radii and mesh refinements under different mixed mode loading conditions obtained with changing the angle β between the loading direction and the notch bisectors line. The error in evaluating the SED value has been obtained comparing the results obtained through a free mesh FE model and a FE model that allows the application of the conventional procedure of the SED method. The main conclusions are the following:

- The application of the SED method does not require an accurate determination of the position of the FPSM, whose coordinates are needed to build the control volume in the right position along the notch fillet, considering that an error in evaluating this position

Table 3
Modeling recommendations to apply the SED method according to the volume free procedure.

3 nodes Plane 182		6 nodes Plane 183	
Suggested mesh size at the notch tip	Expected error %	Suggested mesh size at the notch tip	Expected error %
$3 < min[R_0; \gamma/2]/Size_{averaged} \leq 5$	$|Err\%_{max}| \leq 9\%$	$3 < min[R_0; \gamma/2]/Size_{averaged} \leq 5$	$|Err\%_{max}| \leq 4.5\%$
Notes: not recommended for component subjected to mixed mode conditions			

results in a lower and, in overall, acceptable assessment of the SED value.

- A good approximation of the SED value can be achieved with a free mesh model whose accuracy depends on the mesh refinement defined as the ratio between R_0 or $\gamma/2$ and the $size_{ave.}$ following the criterion explained in section 3, according to which the mesh size at the notch fillet should be defined as a ratio of the minimum between the control volume R_0 and $\gamma/2$.
- With an obtained mesh refinement comprised in the following range $3 < min[R_0; \gamma/2]/Size_{averaged} \leq 5$, the evaluation of the SED value with a free mesh model, as regards the six nodes PLANE 183 element, leads to an average error of zero with a standard deviation not exceeding 1% and with a maximum error, in absolute value, lower than 4.5%.
- The use of the three-node PLANE 182 element results not appropriate to evaluate the SED value in mixed mode conditions with an error that can reach a maximum underestimation of 9%. Depending on the loading conditions the SED value is estimated with a negative average value that decreases, in absolute value, going from mixed mode conditions to mode I condition ($\beta = 90°$).
- A relationship has been noticed between the error in evaluating the SED error and the ratio between the control volume radius and the fillet length R_0/γ: the error in evaluating the SED decreases with decreasing the ratio R_0/γ. According to the authors, this could be a result of a greater difference between the length of the two arcs that define the control volume in comparison to the control volume radius R_0 leading to a better approximation of the control volume shape the mesh size being defined as a ratio of the control volume radius R_0 for the value of the ratio R_0/γ lower than 0.5.

In Table 3, the modeling recommendations for designers applying the SED method are reported based on the results of the present work.

CRediT authorship contribution statement

Pietro Foti: Conceptualization, Methodology, Software, Validation, Formal analysis, Investigation, Data curation, Writing - original draft, Visualization. **Seyed Mohammad Javad Razavi:** Methodology, Writing - review & editing, Supervision. **Majid Reza Ayatollahi:** Writing - review & editing, Supervision. **Liviu Marsavina:** Writing - review & editing, Supervision. **Filippo Berto:** Resources, Writing - review & editing, Supervision, Project administration.

Declaration of Competing Interest

The authors declare that they have no known competing financial interests or personal relationships that could have appeared to influence the work reported in this paper.

References

[1] Fricke W. IIW guideline for the assessment of weld root fatigue. Weld World 2013; 57:753–91. https://doi.org/10.1007/s40194-013-0066-y.
[2] 1993-1-9 EN. Eurocode 3: Design of steel structures-Part 1-9: Fatigue. Eur Comm Stand Brussels, Belgium; 2005.
[3] Hobbacher A. Recommendations for fatigue design of welded joints and components, vol. 47. Springer; 2016.
[4] Radaj D, Sonsino CM, Fricke W. Recent developments in local concepts of fatigue assessment of welded joints. Int J Fatigue 2009;31:2–11. https://doi.org/10.1016/j.ijfatigue.2008.05.019.
[5] Fricke W, Kahl A. Comparison of different structural stress approaches for fatigue assessment of welded ship structures. Mar Struct 2005;18:473–88. https://doi.org/10.1016/j.marstruc.2006.02.001.
[6] Foti P, Filippi S, Berto F. Fatigue assessment of welded joints by means of the strain energy density method: Numerical predictions and comparison with eurocode 3. Frat Ed Integrita Strutt 2019;13. https://doi.org/10.3221/IGF-ESIS.47.09.
[7] Radaj D, Sonsino CM, Fricke W. Fatigue Assessment of Welded Joints by Local Approaches: Second Edition; 2006. https://doi.org/10.1533/9781845691882.
[8] Ayatollahi MR, Rashidi Moghaddam M, Razavi SMJ, Berto F. Geometry effects on fracture trajectory of PMMA samples under pure mode-I loading. Eng Fract Mech 2016;163:449–61. https://doi.org/10.1016/j.engfracmech.2016.05.014.
[9] Ayatollahi MR, Rashidi Moghaddam M, Berto F. A generalized strain energy density criterion for mixed mode fracture analysis in brittle and quasi-brittle materials. Theor Appl Fract Mech 2015;79:70–6. https://doi.org/10.1016/j.tafmec.2015.09.004.
[10] Lazzarin P, Zambardi R. A finite-volume-energy based approach to predict the static and fatigue behavior of components with sharp V-shaped notches. Int J Fract 2001;112:275–98. https://doi.org/10.1023/A:1013595930617.
[11] Lazzarin P, Zambardi R. The equivalent strain energy density approach re-formulated and applied to sharp V-shaped notches under localized and generalized plasticity. Fatigue Fract Eng Mater Struct 2002;25:917–28. https://doi.org/10.1046/j.1460-2695.2002.00543.x.
[12] Berto F, Lazzarin P, Ayatollahi MR. Brittle fracture of sharp and blunt V-notches in isostatic graphite under pure compression loading. Carbon N Y 2013;63:101–16. https://doi.org/10.1016/j.carbon.2013.06.045.
[13] Radaj D, Lazzarin P, Berto F. Fatigue assessment of welded joints under slit-parallel loading based on strain energy density or notch rounding. Int J Fatigue 2009;31: 1490–504. https://doi.org/10.1016/j.ijfatigue.2009.05.005.
[14] Aliha MRM, Berto F, Mousavi A, Razavi SMJ. On the applicability of ASED criterion for predicting mixed mode I+II fracture toughness results of a rock material. Theor Appl Fract Mech 2017;92:198–204. https://doi.org/10.1016/j.tafmec.2017.07.022.
[15] Razavi SMJ, Aliha MRM, Berto F. Application of an average strain energy density criterion to obtain the mixed mode fracture load of granite rock tested with the cracked asymmetric four-point bend specimens. Theor Appl Fract Mech 2018;97: 419–25. https://doi.org/10.1016/j.tafmec.2017.07.004.
[16] Zappalorto M, Carraro PA. An efficient energy-based approach for the numerical assessment of mode I NSIFs in isotropic and orthotropic notched plates. Theor Appl Fract Mech 2020;108:102612. https://doi.org/10.1016/j.tafmec.2020.102612.
[17] Campagnolo A, Zuin S, Meneghetti G. Averaged strain energy density estimated rapidly from nodal displacements by coarse FE analyses: Cracks under mixed mode loadings. Fatigue Fract Eng Mater Struct 2020:1658–85. https://doi.org/10.1111/ffe.13187.
[18] Foti P, Ayatollahi MR, Berto F. Rapid strain energy density evaluation for V-notches under mode I loading conditions. Eng Fail Anal 2020;110. https://doi.org/10.1016/j.engfailanal.2019.104361.
[19] Foti P, Berto F. Evaluation of the strain energy density value without the construction of the control volume in the preprocessing phase of the finite element analysis. Proc Struct Integr, vol. 18; 2019. https://doi.org/10.1016/j.prostr.2019.08.152.
[20] Foti P, Berto F. Strain energy density evaluation with free coarse mesh model. Mater Des Process Commun 2019:1–4. https://doi.org/10.1002/mdp2.116.
[21] Fischer C, Fricke W, Rizzo CM. Experiences and recommendations for numerical analyses of notch stress intensity factor and averaged strain energy density. Eng Fract Mech 2016;165:98–113. https://doi.org/10.1016/j.engfracmech.2016.08.012.
[22] Lazzarin P, Berto F, Zappalorto M. Rapid calculations of notch stress intensity factors based on averaged strain energy density from coarse meshes: Theoretical bases and applications. Int J Fatigue 2010;32:1559–67. https://doi.org/10.1016/j.ijfatigue.2010.02.017.
[23] Lazzarin P, Livieri P, Berto F, Zappalorto M. Local strain energy density and fatigue strength of welded joints under uniaxial and multiaxial loading. Eng Fract Mech 2008;75:1875–89. https://doi.org/10.1016/J.ENGFRACMECH.2006.10.019.
[24] Berto F, Gallo P, Lazzarin P. High temperature fatigue tests of un-notched and notched specimens made of 40CrMoV13.9 steel. Mater Des 2014;63:609–19. https://doi.org/10.1016/j.matdes.2014.06.048.
[25] Razavi SMJ, Ferro P, Berto F, Torgersen J. Fatigue strength of blunt V-notched specimens produced by selective laser melting of Ti-6Al-4V. Theor Appl Fract Mech 2018;97:376–84. https://doi.org/10.1016/j.tafmec.2017.06.021.
[26] Torabi AR, Campagnolo A, Berto F. Local strain energy density to predict mode II brittle fracture in Brazilian disk specimens weakened by V-notches with end holes. Mater Des 2015;69:22–9. https://doi.org/10.1016/j.matdes.2014.12.037.

[27] Berto F, Barati E. Fracture assessment of U-notches under three point bending by means of local energy density. Mater Des 2011;32:822–30. https://doi.org/10.1016/j.matdes.2010.07.017.

[28] Lazzarin P, Berto F, Gomez FJ, Zappalorto M. Some advantages derived from the use of the strain energy density over a control volume in fatigue strength assessments of welded joints. Int J Fatigue 2008;30:1345–57. https://doi.org/10.1016/j.ijfatigue.2007.10.012.

[29] Pook LP, Campagnolo A, Berto F. Coupled fracture modes of discs and plates under anti-plane loading and a disc under in-plane shear loading. Fatigue Fract Eng Mater Struct 2016;39:924–38. https://doi.org/10.1111/ffe.12389.

[30] Berto F, Lazzarin P. Recent developments in brittle and quasi-brittle failure assessment of engineering materials by means of local approaches. Mater Sci Eng R Reports 2014;75:1–48. https://doi.org/10.1016/j.mser.2013.11.001.

[31] Radaj D, Vormwald M. Advanced methods of fatigue assessment. vol. 9783642307. 2013. https://doi.org/10.1007/978-3-642-30740-9.

[32] Berto F, Lazzarin P. Multiparametric full-field representations of the in-plane stress fields ahead of cracked components under mixed mode loading. Int J Fatigue 2013;46:16–26. https://doi.org/10.1016/j.ijfatigue.2011.12.004.

[33] Berto F, Lazzarin P, Wang CH. Three-dimensional linear elastic distributions of stress and strain energy density ahead of V-shaped notches in plates of arbitrary thickness. Int J Fract 2004;127:265–82. https://doi.org/10.1023/B:FRAC.0000036846.23180.4d.

[34] Berto F, Lazzarin P, Matvienko YG. J-integral evaluation for U- and V-blunt notches under Mode I loading and materials obeying a power hardening law. Int J Fract 2007;146:33–51. https://doi.org/10.1007/s10704-007-9134-x.

[35] Radaj D. State-of-the-art review on the local strain energy density concept and its relation to the J-integral and peak stress method. Fatigue Fract Eng Mater Struct 2015;38:2–28. https://doi.org/10.1111/ffe.12231.

[36] Berto F, Lazzarin P, Kotousov A. On higher order terms and out-of-plane singular mode. Mech Mater 2011;43:332–41. https://doi.org/10.1016/j.mechmat.2011.03.004.

[37] Lazzarin P, Lassen T, Livieri P. A notch stress intensity approach applied to fatigue life predictions of welded joints with different local toe geometry. Fatigue Fract Eng Mater Struct 2003;26:49–58. https://doi.org/10.1046/j.1460-2695.2003.00586.x.

[38] Livieri P, Lazzarin P. Fatigue strength of steel and aluminium welded joints based on generalised stress intensity factors and local strain energy values. Int J Fract 2005;133:247–76. https://doi.org/10.1007/s10704-005-4043-3.

[39] Zhu S-P, Yu Z-Y, Correia J, De Jesus A, Berto F. Evaluation and comparison of critical plane criteria for multiaxial fatigue analysis of ductile and brittle materials. Int J Fatigue 2018;112:279–88. https://doi.org/10.1016/j.ijfatigue.2018.03.028.

[40] Berto F, Lazzarin P. Fatigue strength of structural components under multi-axial loading in terms of local energy density averaged on a control volume. Int J Fatigue 2011;33:1055–65. https://doi.org/10.1016/j.ijfatigue.2010.11.019.

[41] Foti P, Berto F. Francis-99: Evaluation of the strain energy density value for welded joints typical of turbine runner blades. J Phys Conf Ser 2019;1296. https://doi.org/10.1088/1742-6596/1296/1/012007.

[42] Foti P, Berto F. Evaluation of the effect of the TIG-dressing technique on welded joints through the strain energy density method. Procedia Struct Integr 2020;25:201–8. https://doi.org/10.1016/j.prostr.2020.04.024.

[43] Foti P, Berto F. Fatigue assessment of high strength welded joints through the strain energy density method. Fatigue Fract Eng Mater Struct 2020;43:2694–702. https://doi.org/10.1111/ffe.13336.

[44] Berto F, Lazzarin P. A review of the volume-based strain energy density approach applied to V-notches and welded structures. Theor Appl Fract Mech 2009;52:183–94. https://doi.org/10.1016/j.tafmec.2009.10.001.

[45] Lazzarin P, Berto F. Some expressions for the strain energy in a finite volume surrounding the root of blunt V-notches. Int J Fract 2005;135:161–85. https://doi.org/10.1007/s10704-005-3943-6.

[46] Lazzarin P, Berto F. From Neuber's elementary volume to Kitagawa and Atzori's diagrams: An interpretation based on local energy. Int J Fract 2005;135:33–8. https://doi.org/10.1007/s10704-005-4393-x.

[47] Yosibash Z, Bussiba A, Gilad I. Failure criteria for brittle elastic materials. Int J Fract 2004;125:307–33. https://doi.org/10.1023/b:frac.0000022244.31825.3b.

[48] Lazzarin P, Sonsino CM, Zambardi R. A notch stress intensity approach to assess the multiaxial fatigue strength of welded tube-to-flange joints subjected to combined loadings. Fatigue Fract Eng Mater Struct 2004;27:127–40. https://doi.org/10.1111/j.1460-2695.2004.00733.x.

[49] Gómez FJ, Elices M, Berto F, Lazzarin P. A generalised notch stress intensity factor for U-notched components loaded under mixed mode. Eng Fract Mech 2008;75:4819–33. https://doi.org/10.1016/j.engfracmech.2008.07.001.

[50] Gómez FJ, Elices M, Berto F, Lazzarin P. Local strain energy to assess the static failure of U-notches in plates under mixed mode loading. Int J Fract 2007;145:29–45. https://doi.org/10.1007/s10704-007-9104-3.

[51] Berto F, Lazzarin P, Gómez FJ, Elices M. Fracture assessment of U-notches under mixed mode loading: Two procedures based on the "equivalent local mode I" concept. Int J Fract 2007;148:415–33. https://doi.org/10.1007/s10704-008-9213-7.

[52] Lazzarin P, Berto F, Ayatollahi MR. Brittle failure of inclined key-hole notches in isostatic graphite under in-plane mixed mode loading. Fatigue Fract Eng Mater Struct 2013;36:942–55. https://doi.org/10.1111/ffe.12057.

[53] Berto F, Lazzarin P, Marangon C. Brittle fracture of U-notched graphite plates under mixed mode loading. Mater Des 2012;41:421–32. https://doi.org/10.1016/j.matdes.2012.05.022.